



PAPER

[View Article Online](#)
[View Journal](#) | [View Issue](#)Cite this: *Catal. Sci. Technol.*, 2018,
8, 3795Elucidating the active sites for CO₂
electroreduction on ligand-protected Au₂₅
nanoclusters†Natalie Austin,^a Shuo Zhao,^b James R. McKone, ^a
Rongchao Jin^b and Giannis Mpourmpakis ^{*a}

Using density functional theory (DFT) calculations, we investigated the electrochemical reduction of CO₂ and the competing H₂ evolution reaction on ligand-protected Au₂₅ nanoclusters (NCs) of different charge states, Au₂₅(SR)₁₈^q ($q = -1, 0, +1$). Our results showed that regardless of charge state, CO₂ electroreduction over Au₂₅(SR)₁₈^q NCs was not feasible because of the extreme endothermicity to stabilize the carboxyl (COOH) intermediate. When we accounted for the removal of a ligand (both –SR and –R) from Au₂₅(SR)₁₈^q under electrochemical conditions, surprisingly we found that this is a thermodynamically feasible process at the experimentally applied potentials with the generated surface sites becoming active centers for electrocatalysis. In every case, the negatively charged NCs, losing a ligand from their surface during electrochemical conditions, were found to significantly stabilize the COOH intermediate, resulting in dramatically enhanced CO₂ reduction. The generated sites for CO₂ reduction were also found to be active for H₂ evolution, which agrees with experimental observations that these two processes compete. Interestingly, we found that the removal of an –R ligand from the negatively charged NC, resulted in a catalyst that was both active and selective for CO₂ reduction. This work highlights the importance of both the overall charge state and generation of catalytically active surface sites on ligand-protected NCs, while elucidating the CO₂ electroreduction mechanisms. Overall, our work rationalizes a series of experimental observations and demonstrates pathways to convert a very stable and catalytically inactive NC to an active electrocatalyst.

Received 29th May 2018,
Accepted 29th June 2018

DOI: 10.1039/c8cy01099d

rsc.li/catalysis

Introduction

Growing fossil fuel consumption to meet energy demands has led to rising CO₂ emissions, which could have detrimental effects on the environment if left unmitigated.¹ There is an emerging interest in electrocatalysis as a route to reduce CO₂ emissions by sustainably converting CO₂ to useful chemicals and fuels.^{2–6} Electrochemical conditions are advantageous for this reaction because applied potentials can be used to drive the reduction at ambient pressures and temperatures, and the electricity required to reduce CO₂ can be acquired from renewable resources such as wind and solar power.^{7–11} Presently, the challenge with reducing CO₂ electrocatalytically is that it is not industrially feasible due to the highly reducing potentials required to obtain desired products such as hydrocarbons and CO.^{7,12,13} Additionally, at these extreme potentials, there is low

selectivity for desired products due to the competing H₂ evolution reaction.^{8,14} Therefore, there is continued interest in the design of active catalysts that promote CO₂ reduction at modest potentials while minimizing hydrogen evolution.

Experimental work by Hori *et al.* demonstrated that bulk Au electrodes can successfully reduce CO₂ to CO.^{13,15} Additional studies have shown that nanosized Au electrodes are more active than bulk Au electrodes.^{16–18} The enhanced activity of Au nanoparticles (NPs) has been attributed to catalyst properties such as high surface area and increased presence of low-coordinated sites that strongly bind reaction intermediates.^{17,19–21} Mistry *et al.* investigated CO₂ reduction on Au NPs 1.1 nm to 7.7 nm in size. The authors identified that NPs below 5 nm were significantly more active than bulk Au whereas, NPs larger than 5 nm were comparably active to bulk Au. The activity of the Au NPs less than 5 nm in size was attributed to the presence of low-coordinated sites such as corners and edges. Interestingly, the catalytically more active and smaller NPs (<5 nm) were more selective towards H₂.¹⁶ Hall *et al.* showed that porous Au film thickness (ranging from 0.5 to 2.7 μm) can also influence CO₂ reduction selectivity.²² The authors observed a suppression in hydrogen evolution with increase in film thickness, leading to increased

^a Department of Chemical Engineering, University of Pittsburgh, Pittsburgh, PA 15261, USA. E-mail: gmpourmp@pitt.edu^b Department of Chemistry, Carnegie Mellon University, Pittsburgh, PA 15213, USA

† Electronic supplementary information (ESI) available. See DOI: 10.1039/c8cy01099d

selectivity towards CO. Thus, in addition to the presence of low-coordinated sites, mass transport effects could also play a role in resulting activity and selectivity of Au NPs for the CO₂ reduction reaction.

In contrast to polydisperse Au NPs, atomically precise Au nanoclusters (NCs), stabilized by organic ligands, exhibit well-defined structure which make them attractive for catalytic applications.^{23,24} However, the presence of ligands can also limit the accessibility of reactants to Au sites resulting in reduced catalyst activity.^{25–27} Despite this, Kauffman *et al.*, has observed enhanced catalytic activity of ligand-protected NCs compared to unprotected NPs at reducing potentials as small as -0.193 V.¹⁸ Specifically, the authors compared the activity of a fully ligand-protected Au₂₅(SC₂H₄Ph)₁₈[–] NC, about 1 nm in size, to unprotected (metallic) 2 nm and 5 nm Au NPs, and bulk Au. Despite the small size of the Au₂₅(SC₂H₄Ph)₁₈[–] NC, contrary to Mistry *et al.*,¹⁶ the NC was more selective towards CO than the NPs and bulk Au. In addition, the Au₂₅(SC₂H₄Ph)₁₈[–] NC produced peak CO production at -1.0 V vs. RHE, at a rate 7–700 times higher than on the NPs and bulk Au. This suggests that the ligands designed to stabilize these Au NCs have an effect in the selective reduction of CO₂ to CO. Despite the negative potentials applied, a retention of the optical spectra before and after CO₂ reduction suggests that the Au₂₅(SC₂H₄Ph)₁₈[–] NC did not change size, and that the S–Au–S–Au–S bonding motif in the cluster shell was majorly retained. The potential scalability and long-term performance of electroreduction of CO₂ over the Au₂₅(SC₂H₄Ph)₁₈[–] NC has also been investigated.²⁸ Under realistic on-demand catalyst usage, CO selectivities and Faradaic efficiencies greater than 90%, were achieved through both potentiostat-controlled and renewable solar powered electrolysis. Thus, these ligand-protected Au NCs appear to be attractive electrocatalysts for feasible conversion of CO₂.

Theoretical methods combined with experiments can be used to provide atomic level insight into the catalyst properties that influence CO₂ reduction activity over Au₂₅ NCs. For instance, Kauffman *et al.* assessed CO₂ reduction on fully ligand-protected Au₂₅(SR)₁₈^q NCs in three different charge states ($q = -1, 0, +1$) using DFT calculations and experiments, wherein thiolate ligands were simulated with methylthiols in calculations.²⁹ The negatively charged NC was able to produce more CO from CO₂ reduction than the neutral and positive NCs between -0.7 V and -1.3 V vs. RHE. The activity of Au₂₅(SCH₃)₁₈[–] for CO₂ reduction was computationally attributed to the stabilization of co-adsorbed CO₂ and H⁺ reactants more favorably than on Au₂₅(SCH₃)₁₈^q ($q = 0, +1$). Such a stabilization is expected due to the electrostatic interactions between the negatively charged NC and the proton. The presence of ligand-removed NCs, due to the very negative potentials applied, was not considered in this work, nor the detailed reaction path. In a latter study, Alfonso *et al.* used DFT to investigate CO₂ reduction to CO on fully ligand-protected Au₂₅(SCH₃)₁₈[–] and partially ligand-removed Au₂₅(SCH₃)₁₇[–].³⁰ The authors identified that the COOH species, an important intermediate in CO₂ reduc-

tion, was more stabilized on Au₂₅(SCH₃)₁₇[–] ($\Delta G[*\text{COOH}]$: 0.34 eV) than on Au₂₅(SCH₃)₁₈[–] ($\Delta G[*\text{COOH}]$: 2.04 eV). The stabilization of the COOH intermediate, was attributed to its interaction with exposed Au atoms from the thiol ligand-removed site.³⁰ The investigation of ligand-removed Au₂₅(SCH₃)₁₇[–] was supported using work by Wu *et al.* in which the authors observed an enhancement in CO conversion over the Au₂₅(SC₂H₄Ph)₁₈ NC when thiol-based ligands were removed from the NC.²⁷ In our very recent study on the CO₂ electroreduction on sphere and rod-like ligand-protected Au NCs, we computationally showed that ligand removal can occur under electrochemical conditions and the generated sites exhibited CO₂ electroreduction trends that were observed in experiments.³¹

Results to date illustrate that there is no consensus on the identity of active sites on ligand-protected Au nanocatalysts. Some studies have proposed that under reaction conditions these catalysts remain fully ligand-protected^{18,29,32–34} while others have stated that some ligand removal is necessary for activity to be observed.^{25,27,31,35–39} Additionally, there are competing claims on whether Au nanocatalysts are more selective towards CO (ref. 18, 28 and 40) or H₂ (ref. 16 and 41) under CO₂ reduction conditions. This lack of agreement on the selectivity of Au nanocatalysts, in addition to the elusive active sites under electrocatalytic conditions, make it very difficult to identify chemical strategies for the design and synthesis of thiolated Au NCs that efficiently reduce CO₂. Theoretical studies can give valuable insights into the reaction mechanisms and reveal active catalytic sites, but there are presently very few studies that have investigated the CO₂ reduction behavior on these ligand-protected NCs.^{18,29–31}

Herein, we report a systematic analysis of how the NC charge state and ligand-removal concertedly influence the reaction energetics of the CO₂ reduction and H₂ evolution reactions, by using DFT calculations. This work elucidates the active sites on the NC catalyst surface for CO₂ reduction and provides insight into the mechanisms of their generation that would lead to the design of more efficient CO₂ electroreduction catalysts.

Computational methods

DFT calculations in this study were carried out using the PBE⁴² functional and the double- ζ plus polarization (DZVP) basis set⁴³ with a 500 Ry cutoff in combination with the Goedecker, Teter, and Hutter (GTH) pseudopotentials,⁴⁴ as implemented in the computational package CP2K.⁴⁵ This combination of DFT parameters (functional, pseudopotentials, and basis set) has been successfully used to investigate reaction energetics on Au-based catalysts.^{46–50} The initial geometries of the NCs were generated from experimentally-derived crystallographic data of the Au₂₅(SC₂H₄Ph)₁₈[–] NC.⁵¹ The ligands of the Au₂₅ NC were represented by methylthiolate groups (–SCH₃) generating the Au₂₅(SCH₃)₁₈ NC. Simplification of the ligands, from –SC₂H₄Ph to –SCH₃, is a typical approach used to reduce

computational cost while maintaining the structural integrity of the NCs.^{18,29,30,35,52} As shown in Fig. 1, the $\text{Au}_{25}(\text{SCH}_3)_{18}^q$ NC is composed of a Au_{13} icosahedral core protected by a shell network of six $\text{Au}_2(\text{SCH}_3)_3$ units. The geometries of the NCs were optimized in a $30 \times 30 \times 30 \text{ \AA}^3$ non-periodic cell until the forces were less than 0.02 eV \AA^{-1} . All systems with an even number of electrons had a singlet multiplicity and all systems with an odd number of electrons in this study had a doublet multiplicity (see ESI† Table S1 for more details). The energetics for ligand removal, CO_2 reduction, and H_2 evolution were calculated using thermodynamic methods where the zero-point energy (ZPE), heat capacity (C_p), and entropic (TS) terms were added to the electronic energy (E) as follows: $\Delta G = \Delta E + \Delta \text{ZPE} + \int C_p dT - TS$. Additionally, the computational hydrogen electrode model (CHE)^{12,53} was applied to represent the free energy of a proton (H^+) and electron (e^-) pair in reduction reactions and thereby, calibrate the calculated free energy on an electrochemical scale. Thus, the total free energy for a proton-electron pair with an applied potential (U) is defined as $G(\text{H}^+ + \text{e}^-) = G(1/2\text{H}_2) - neU$ where n is the number of electrons transferred and e is the electronic charge. Gas phase corrections as calculated by Peterson *et al.*, were also applied to the electronic energies of the gaseous molecules.¹² For the free energies of the adsorbates the vibrational components of the heat capacity and entropic terms were considered. The vibrational modes of the adsorbates were determined by keeping the optimized NC fixed and computing the frequencies of the adsorbate within the harmonic oscillator approximation. This approach has been successfully applied using DFT in electrocatalysis,^{19,30,54,55} including $\text{Au}_{25}(\text{SCH}_3)_{18}$. The computationally predicted limiting potential (U_l)^{12,56} was calculated as the applied potential required for the rate determining step, to become thermoneutral ($\Delta G = 0$).

The Au_{25}^q NC which has been stably synthesized in multiple charge states ($q = -1, 0, +1$)^{57–59} has also been used for catalysis in each of the charge states.²⁹ In the ESI† (Table S2) we assess the relative stability of the Au_{25} NC in relation to the charge states using adiabatic electron affinity (AEA),

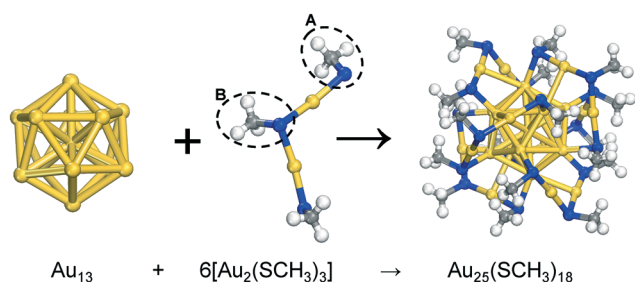


Fig. 1 Schematic of the fully-ligand protected $\text{Au}_{25}(\text{SCH}_3)_{18}$ NC. The system is composed of a Au_{13} icosahedral core protected by a shell network of six $\text{Au}_2(\text{SR})_3$ units. The Au, S, C, and H atoms are colored yellow, blue, grey, and white, respectively. The labels “A” and “B” on the $\text{Au}_2(\text{SCH}_3)_3$ shell network represent the two distinct types of coordinated sulfur in the NC shell.

$\text{Au}_{25}(\text{SCH}_3)_x^0 + \text{e}^- \rightarrow \text{Au}_{25}(\text{SCH}_3)_x^-$ and adiabatic ionization potential (AIP, $\text{Au}_{25}(\text{SCH}_3)_x^0 \rightarrow \text{Au}_{25}(\text{SCH}_3)_x^+ + \text{e}^-$).^{60,61} Studies have also suggested that under reaction conditions, the Au_{25} NC can partially lose ligands.^{27,30} Therefore we calculate the energy required to remove ligands from the $\text{Au}_{25}(\text{SCH}_3)_{18}$ NC. We initially focus on the removal of $-\text{SR}$ ($-\text{SCH}_3$) from the $6[\text{Au}_2(\text{SCH}_3)_3]$ shell of the fully ligand-protected NC in each different charge state. The removal of a $-\text{SR}$ ligand would expose an Au atom and enable interaction with adsorbates. However, theoretical studies on CO_2 reduction on Ni-Fe-S cubanes⁵⁴ and MoS_2 (ref. 62) catalysts have shown that the COOH intermediate can be stabilized more favorably on the S atoms of the catalysts compared to other available sites. Thus, we also considered removal of $-\text{R}$ ($-\text{CH}_3$) from the Au_{25} NCs to expose an S atom to the reaction intermediates for CO_2 reduction to CO.

The ΔG for ligand removal of $-\text{SR}$ from $\text{Au}_{25}(\text{SCH}_3)_{18}$ was calculated as an electrochemical reduction step, using eqn (1), which was derived according to the following reduction reaction: $\text{Au}_{25}(\text{SCH}_3)_{18}^q + \text{H}^+ + \text{e}^- \rightarrow \text{HSCH}_3 + \text{Au}_{25}(\text{SCH}_3)_{17}^q$.

$$\Delta G_{\text{methylthiol-removal}} = G[\text{Au}_{25}(\text{SCH}_3)_{17}]^q + G[\text{HSCH}_3] - G[\text{Au}_{25}(\text{SCH}_3)_{18}]^q - 1/2G[\text{H}_2] + neU \quad (1)$$

where $G[\text{Au}_{25}(\text{SCH}_3)_{17}]$, $G[\text{HSCH}_3]$, $G[\text{Au}_{25}(\text{SCH}_3)_{18}]$, and $G[\text{H}_2]$ are the gas phase free energies of the isolated NC with a removed thiol, the HSCH_3 molecule, the fully ligand-protected NC, and the H_2 molecule, respectively. The ΔG for removal of $-\text{R}$ was calculated in the same manner as for $-\text{SR}$ with $G[\text{Au}_{25}(\text{SCH}_3)_{17}]^q$ and $G[\text{HSCH}_3]$ in eqn (1) being replaced by $G[\text{Au}_{25}\text{S}(\text{SCH}_3)_{17}]^q$ and $G[\text{CH}_4]$, respectively. All vibrational modes were considered in the analysis of free energies of ligand removal. An overview of the potential states of the Au_{25}^q NC under reaction conditions that we consider in this study are shown in Fig. 2 (shown for $-\text{SCH}_3$ removal).

Prior studies have suggested^{12,17,30} that CO_2 reduction and hydrogen evolution can take place through the following steps:

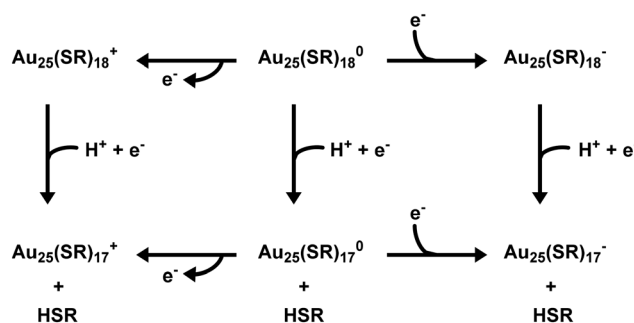
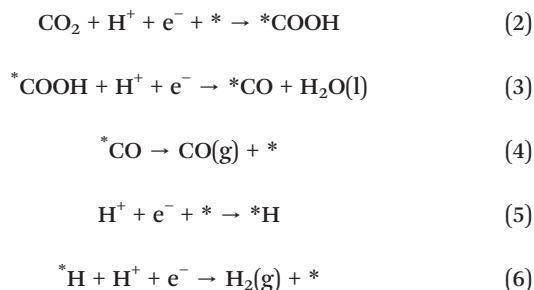


Fig. 2 A cycle which illustrates potential states of the Au_{25} NC under reaction conditions. The top and bottom rows, show electron transfer to form the fully ligand-protected and partially ligand removed NCs in each charge state, respectively. The vertical steps indicate ligand removal from $\text{Au}_{25}(\text{SR})_{18}^q$ to form $\text{Au}_{25}(\text{SR})_{17}^q$.



An example for determining reaction energetics using the first step of CO₂ reduction on the NCs (2), is calculated as follows:

$$\Delta G_{* \text{COOH}} = G[\text{COOH}^*] - G[\text{NC}] - G[\text{CO}_2] - 1/2 G[\text{H}_2] + neU \quad (7)$$

where $G[\text{COOH}^*]$, $G[\text{NC}]$, $G[\text{CO}_2]$, $G[\text{H}_2]$ are the gas phase free energies of the COOH adsorbed on a NC, the NC, the CO₂ molecule, and the H₂ molecule, respectively. In the ESI† (Fig. S1) we also assessed CO₂ adsorption on the NCs and observed only physisorbed CO₂ as previously reported.¹⁸

Results

DFT geometry optimizations illustrated that the final structures of the fully ligand-protected Au₂₅(SR)₁₈^q ($q = -1, 0, +1$) NCs are nearly structurally identical to the experimental crystal structure.^{29,57,59,63} The calculated free energy diagrams for CO₂ reduction and H₂ evolution on the fully ligand-protected Au₂₅(SCH₃)₁₈^q NCs ($q = -1, 0, +1$), at $U = 0$ V (solid lines) are shown in Fig. 3. The ΔG values of the reactions were also evaluated at an applied potential of -1.0 V vs. RHE ($U = -1.0$ V,

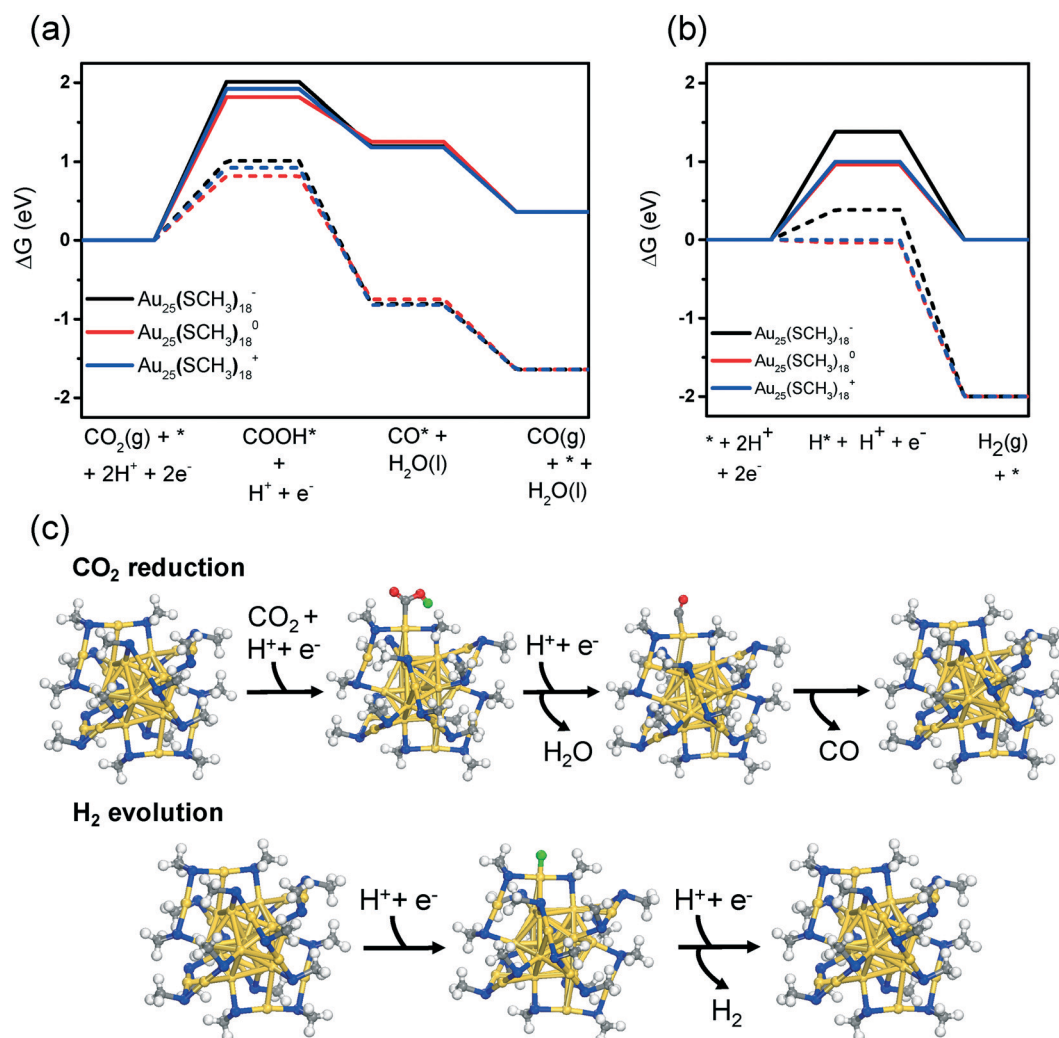


Fig. 3 Free energy diagrams (ΔG) for the (a) reduction of CO₂ to CO and (b) hydrogen evolution on the fully ligand-protected Au₂₅(SCH₃)₁₈^q ($q = -1, 0, +1$) NCs. The black, red, and blue lines represent the energy diagrams generated using a NC in the -1 , 0 , and $+1$ charge states, respectively. The solid lines illustrate the energy diagrams at $U = 0$ V, while the dashed lines represent the energy diagrams at an applied potential of $U = -1.0$ V. (c) Illustrations of the CO₂ reduction and the hydrogen evolution reactions. The Au, S, C, and O, atoms are colored yellow, blue, grey, and red, respectively. The H atoms are white, except for H on the carboxyl (in CO₂ reduction) and the adsorbed H (in hydrogen evolution) which are colored lime green for clarity.

dashed lines in Fig. 3), the potential at which peak production of CO was observed in experimental studies on the NCs.^{18,28} As shown in Fig. 3a, CO₂ reduction to CO on the fully ligand-protected NCs Au₂₅(SCH₃)₁₈ in each charge state, appears to be unfavorable due to the largely endergonic step for COOH stabilization ($\Delta G > 1.82$ eV). The observed unfavorable ΔG^* (COOH), agrees with previous computational observations by Alfonso *et al.*, for CO₂ reduction on the Au₂₅(SCH₃)₁₈[−] NC.³⁰ Although for the hydrogen evolution reaction at $U = 0$ V, the H adsorption step is also endergonic (Fig. 3b), the ΔG for the H adsorption (eqn (5)) is more favorable than the COOH adsorption (eqn (2)). Furthermore, at $U = -1.0$ V, the hydrogen evolution reaction becomes exergonic on the Au₂₅(SCH₃)₁₈^q ($q = 0, +1$) NCs. Overall, the large positive ΔG values for CO₂ reduction on the fully ligand-protected NCs suggest that the production of CO is not feasible on these NCs. Thus, we focused on partially ligand-removed NCs, which have been experimentally shown to be active catalysts.^{27,35–39}

Fig. 4a illustrates partial ligand removal from the Au₂₅(SCH₃)₁₈ NC *via* a reduction reaction. We focus on removing one −SCH₃ ligand, connected to a core Au atom of the NC (labeled in Fig. 1 as site “A” and also shown in Fig. 4a), as has been done in previous studies.³⁰ It should be noted that removing −SCH₃ from site “A” in Fig. 1 is more energetically favorable than from site “B” (see Fig. S2 in the ESI†). In the resulting partially ligand-removed Au₂₅(SCH₃)₁₇ NC, the Au atom of the shell, which was previously bound to the removed −SCH₃ ligand, is now connected to an Au atom of the core. According to our geometry optimization calculations, aside from the site where the −SCH₃ ligand was removed, the Au₂₅(SCH₃)₁₇^q NCs remain geometrically similar to the Au₂₅(SCH₃)₁₈^q NC. To assess the ability of the Au₂₅(SCH₃)₁₈^q NCs to release a −SCH₃ ligand, we calculated the ΔG for the electrochemical step of Au₂₅(SCH₃)₁₇^q formation from

Au₂₅(SCH₃)₁₈^q as shown in Fig. 4b. The observed trend in ΔG for removing a ligand from Au₂₅(SCH₃)₁₈^q at $U = 0$ V and -1.0 V is as follows (from most favorable to least favorable): Au₂₅(SCH₃)₁₈⁰ < Au₂₅(SCH₃)₁₈⁺ < Au₂₅(SCH₃)₁₈[−]. This trend follows the order of increasing stability of the fully ligand-protected NCs as depicted on the increasing HOMO–LUMO gaps, calculated by Akola *et al.*⁶⁴ At $U = 0$ V the formation of the partially ligand-removed Au₂₅(SCH₃)₁₇^q NCs is less endergonic than the COOH adsorption on the fully ligand-protected Au₂₅(SCH₃)₁₈^q NCs. Interestingly, at $U = -1.0$ V, the ΔG for Au₂₅(SCH₃)₁₇ formation becomes exergonic in each charge state, as shown by the dashed lines in Fig. 4b. Thus, under reaction conditions (-1.0 V vs. RHE) calculations clearly predict the formation of partially ligand-removed catalysts.

Following the observation of exergonic ΔG for Au₂₅(SCH₃)₁₇^q formation at $U = -1.0$ V, we assessed CO₂ reduction and H₂ evolution on the Au₂₅(SCH₃)₁₇^q NCs ($q = -1, 0, +1$). As shown in Fig. 5a, we found that the partially ligand-removed NCs better stabilized the COOH intermediate ($\Delta G < 1.42$ eV) relative to the fully ligand-protected NCs ($\Delta G > 1.82$ eV). Thus, in each charge state the presence of ligand-removed sites on the NCs enhances COOH surface stabilization compared to the fully ligand-protected NCs. The lower ΔG^* (COOH) observed on the Au₂₅(SCH₃)₁₇^q NCs suggests that ligand removal is important for the Au NCs to become active, as highly endergonic free energies were observed on the fully ligand-protected NCs even with an applied potential ($U = -1.0$ V). The Au₂₅(SCH₃)₁₇[−] NC had the least endergonic ΔG^* (COOH) compared to Au₂₅(SCH₃)₁₇^q ($q = 0, +1$) at $U = 0$ V, which is conceptually consistent with the Lewis acidity of CO₂. Thus, we would expect the partially ligand-removed NCs to be most active in a negative charge state. Given the exergonic ΔG^* (H) shown in Fig. 5b, we would also expect competition with H₂ evolution on partially

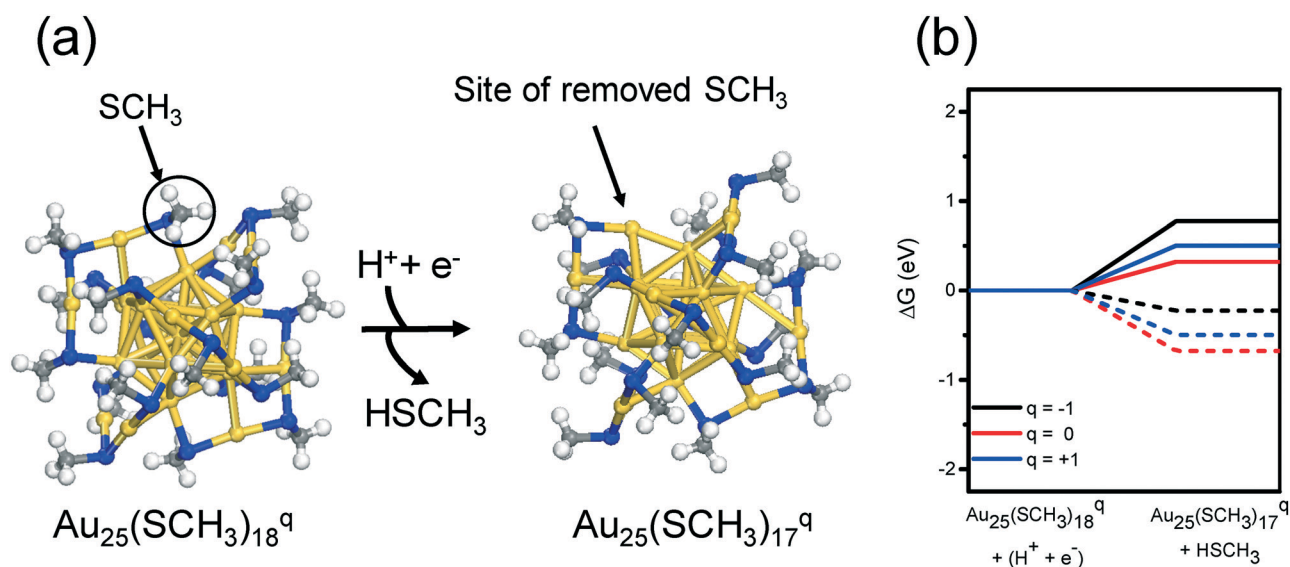


Fig. 4 (a) Schematic for the reduction of the fully ligand-protected NCs (Au₂₅(SCH₃)₁₈^q) to partially ligand-removed Au₂₅(SCH₃)₁₇^q. The color code is as shown in Fig. 3. (b) Free energy diagram for removing one −SCH₃ from the NC. As described in Fig. 3, the colored, solid, and dashed lines represent the different charge states and energetics at $U = 0$ V and at $U = -1.0$ V, respectively.

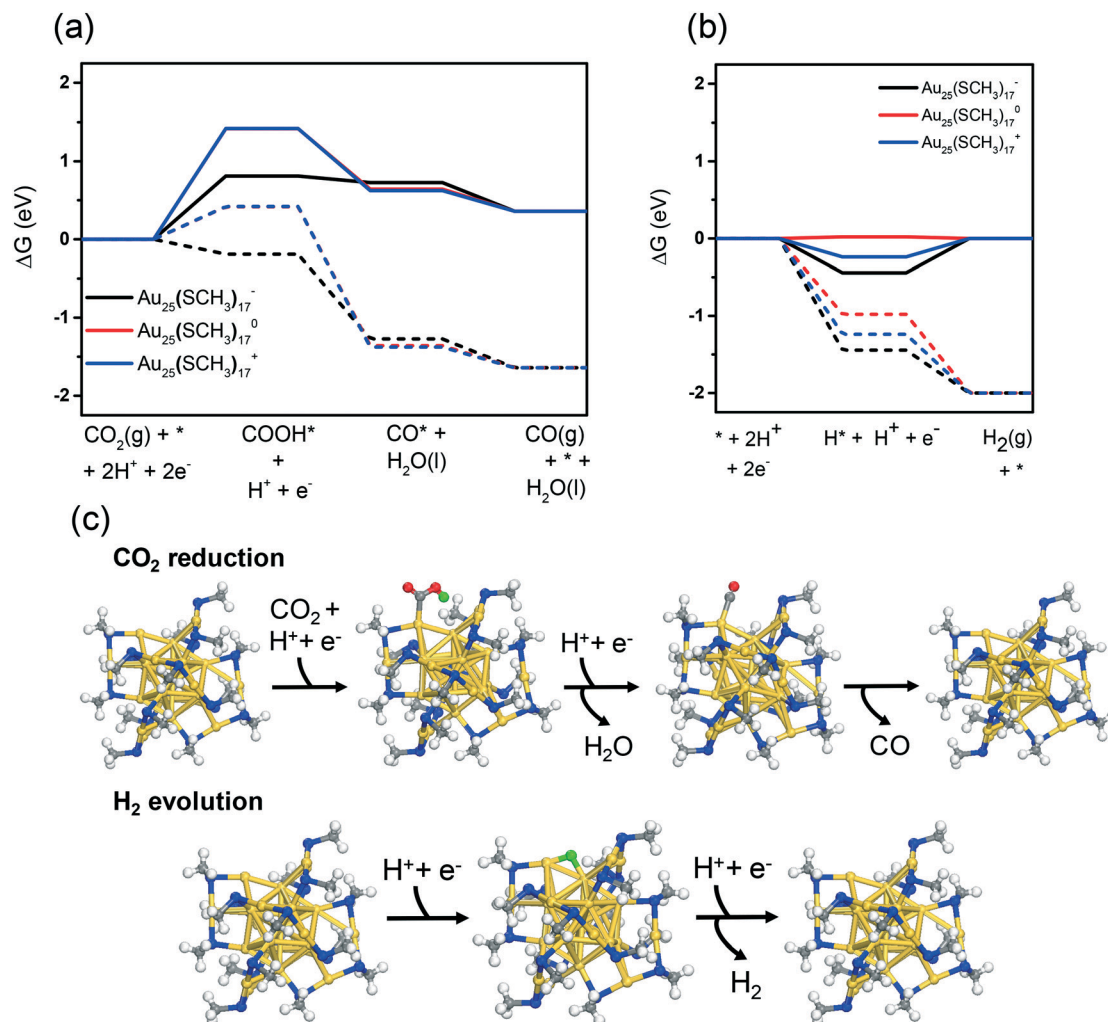


Fig. 5 Free energy diagrams (ΔG) for the (a) reduction of CO₂ to CO and the (b) hydrogen evolution reaction on the Au₂₅(SCH₃)₁₇^q ($q = -1, 0, +1$) NCs (with a ligand removed). (c) Illustrations of CO₂ reduction and H₂ evolution reaction steps. The color code for the diagrams is as described in Fig. 3.

ligand-removed NCs. It should be noted that adsorbate interactions can be influenced by solvation.⁵⁶ Thus, in the ESI† (Fig. S3) we assessed the H₂O solvent effect on CO₂ reduction and H₂ evolution energetics on the Au₂₅(SCH₃)₁₇⁻ NC. The results showed an enhancement in stabilizing the COOH intermediate in the presence of H₂O. Additionally, the trends observed without solvation (*i.e.* competition with H₂ evolution), remained in the solvated case studied.

Having shown that the ligand removal on the NCs can generate active sites for CO₂ electroreduction and knowing that catalysts with surface sulfur atoms, such as Ni-Fe-S cubanes⁵⁴ and MoS₂,⁶² stabilize the COOH intermediate in CO₂ reduction, we investigated the removal of -CH₃ from the Au₂₅(SCH₃)₁₈ NC to generate a surface sulfur site instead of a bare Au site (Fig. 6a). Similarly, to -SCH₃ removal, we focus on removing -CH₃ from site "A" as indicated in Fig. 1, in each charge state of the Au₂₅ NC. The observed trend for removing a -CH₃ from Au₂₅(SCH₃)₁₈^q at $U = 0$ V and -1.0 V is the same as removing -SCH₃ from Au₂₅(SCH₃)₁₈^q: Au₂₅(SCH₃)₁₈⁰ < Au₂₅(SCH₃)₁₈⁺ < Au₂₅(SCH₃)₁₈⁻ (from most favorable to least

favorable). Remarkably, unlike the endergonic ΔG observed for -SCH₃ removal at $U = 0$ V, the ΔG for -CH₃ removal is exergonic in each charge state. Thus, under reaction conditions (-1.0 V vs. RHE) calculations predict that bare Au sites (due to -SCH₃ removal) and S sites (due to -CH₃ removal) may coexist. However, we note that we have not assessed here the free energies for ligand removal associated with an experimentally utilized ligand (*i.e.* -SC₂H₄Ph) due to computational constraints. However, in the ESI† (Fig. S4) we present an energy analysis comparing -SC₂H₄Ph removal to -C₂H₄Ph removal in the negatively charged state of the Au₂₅ NC. These results indicate that under reaction conditions the formation of the partially-ligand removed NCs is still plausible.

Due to the preferable $\Delta G(*\text{COOH})$ on Au₂₅(SCH₃)₁₇⁻ relative to Au₂₅(SCH₃)₁₇^q ($q = 0, +1$), we examine CO₂ reduction and H₂ evolution on the Au₂₅S(SCH₃)₁₇⁻ NC (-CH₃ removed) and compare the energetics to the Au₂₅(SCH₃)₁₇⁻ NC (-SCH₃ removed). As shown in Fig. 7a, we found that Au₂₅S(SCH₃)₁₇⁻ stabilizes COOH more favorably ($\Delta G(*\text{COOH}) = 0.33$ eV) relative to Au₂₅(SCH₃)₁₇⁻ ($\Delta G(*\text{COOH}) = 0.81$ eV). This enhanced

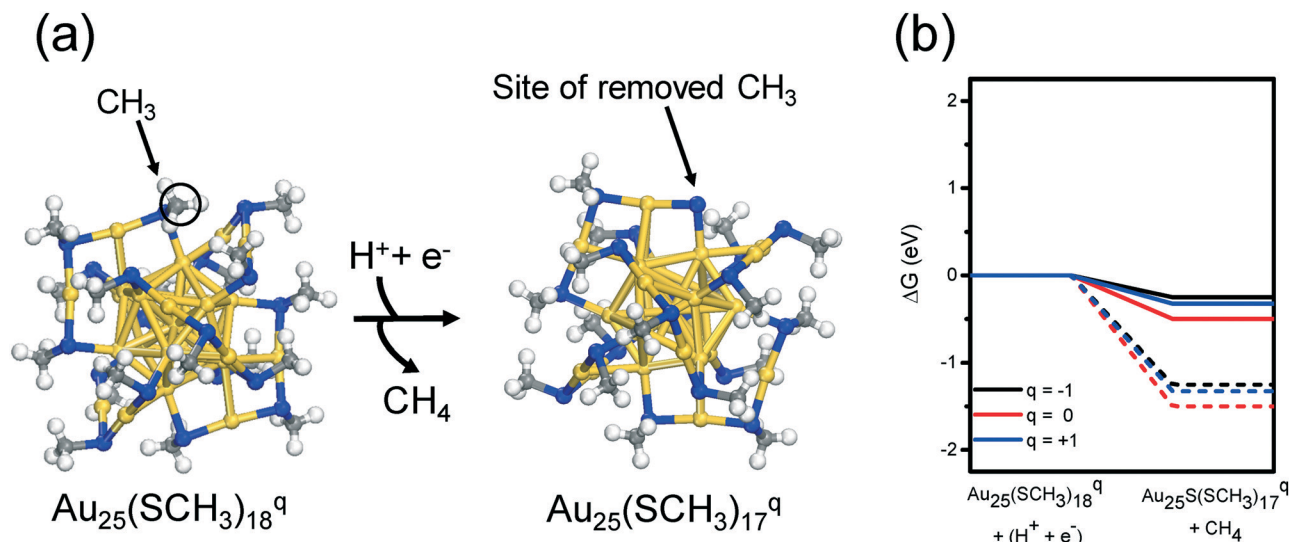


Fig. 6 (a) Schematic for the reduction of the fully ligand-protected NC ($\text{Au}_{25}(\text{SCH}_3)_{18}^q$) to one with $-\text{CH}_3$ removed, $\text{Au}_{25}\text{S}(\text{SCH}_3)_{17}^q$. The color code is as shown in Fig. 3. (b) Free energy diagram for removing one $-\text{CH}_3$ from the NC. As described in Fig. 3, the colored, solid, and dashed lines, represent the charge states, the energetics at $U = 0$ V and at $U = -1.0$ V, respectively.

COOH adsorption could be attributed to the larger negative charge on the exposed S site of the $\text{Au}_{25}\text{S}(\text{SCH}_3)_{17}^-$ compared to the exposed Au site of the $\text{Au}_{25}(\text{SCH}_3)_{17}^-$ NC (see ESI† Fig. S5). In addition, the exposed S site of the $\text{Au}_{25}\text{S}(\text{SCH}_3)_{17}^-$ NC contributes to increased electron density near the Fermi level of the $\text{Au}_{25}\text{S}(\text{SCH}_3)_{17}^-$ NC compared to the fully protected $\text{Au}_{25}(\text{SCH}_3)_{18}^-$, which in turn contributes to the reactivity of the NC (see ESI† Fig. S6). In Fig. 7b, we also observe that H adsorption at $U = 0$ V is more exergonic on $\text{Au}_{25}\text{S}(\text{SCH}_3)_{17}^-$ than on $\text{Au}_{25}(\text{SCH}_3)_{17}^-$. This indicates that H_2 evolution would compete with CO_2 reduction on $\text{Au}_{25}\text{S}(\text{SCH}_3)_{17}^-$ NCs.

Determining the selectivity between CO_2 reduction and hydrogen evolution would typically require an in depth kinetic analysis. However, to give a qualitative estimate of the selectivity we determine the difference between the limiting potentials for CO_2 reduction and H_2 evolution ($U_L(\text{CO}_2) - U_L(\text{H}_2)$).^{62,65,66} The more positive $U_L(\text{CO}_2) - U_L(\text{H}_2)$ corresponds to a higher selectivity towards CO_2 reduction relative to the set of NCs. As shown in Table 1, on the $\text{Au}_{25}(\text{SCH}_3)_{18}^q$ and $\text{Au}_{25}(\text{SCH}_3)_{17}^q$ NCs, the limiting step which determines $U_L(\text{CO}_2)$ is the COOH formation step. However, on the $\text{Au}_{25}\text{S}(\text{SCH}_3)_{17}^-$ NC, the limiting step is CO (and H_2O) formation, which results in the smallest $|U_L(\text{CO}_2)|$ amongst all of the nanoclusters in this study. H adsorption is the limiting step that determines $U_L(\text{H}_2)$ on the $\text{Au}_{25}(\text{SCH}_3)_{18}^q$ and the $\text{Au}_{25}(\text{SCH}_3)_{17}^0$ NCs, while the formation of $\text{H}_2(\text{g})$ is the limiting step responsible for $U_L(\text{H}_2)$ on the $\text{Au}_{25}(\text{SCH}_3)_{17}^q$ ($q = +1, -1$) and $\text{Au}_{25}\text{S}(\text{SCH}_3)_{17}^-$ NCs due to the exothermic H adsorption on the NCs. In Fig. 8, the calculated $U_L(\text{CO}_2) - U_L(\text{H}_2)$ shows that the negatively charged species, $\text{Au}_{25}(\text{SCH}_3)_{18}^-$, $\text{Au}_{25}(\text{SCH}_3)_{17}^-$, and $\text{Au}_{25}\text{S}(\text{SCH}_3)_{17}^-$ are the least selective towards H_2 production relative to the set of NCs. Although our results show that only the partially-ligand removed clusters, $\text{Au}_{25}(\text{SCH}_3)_{17}^-$ and

$\text{Au}_{25}\text{S}(\text{SCH}_3)_{17}^-$, are most active for CO_2 reduction, it is only the $\text{Au}_{25}\text{S}(\text{SCH}_3)_{17}^-$ NC which is selective to CO_2 reduction over H_2 evolution (positive value of $U_L(\text{CO}_2) - U_L(\text{H}_2)$). Therefore, the exposure of S atoms, within the NCs are important to tune selectivity towards CO_2 reduction. In experiments, the conditions that control the selectivity of the Au_{25} catalyst towards CO include applied potentials, CO_2 flow rate, catalyst loading, and concentration of the electrolyte.^{28,67} These Au_{25} catalysts are also clearly active toward H_2 evolution. Zhao *et al.*, showed that an $\text{Au}_{25}/\text{MoS}_2$ system enhanced the hydrogen evolution reaction activity compared to MoS_2 alone.⁶⁸ This enhanced activity was attributed to the electronic interactions at the Au- MoS_2 interface. Therefore, these Au NCs can display exceptional but different catalytic behavior depending on the chemical environment. The observed differences in catalytic behavior with changes to NC structure (fully-protected vs. partially-ligand removed) shown in this study can be connected to the frontier orbitals HOMO-LUMO of the clusters (see ESI† Fig. S7). As shown in Fig. S7(a),† the HOMO-LUMO gap of the NCs with a removed ligand becomes much smaller compared to the fully protected NC. In addition, the electron density observed on the ligand removed sites of $\text{Au}_{25}(\text{SCH}_3)_{17}^-$ and $\text{Au}_{25}\text{S}(\text{SCH}_3)_{17}^-$ becomes more localized and directional compared to $\text{Au}_{25}(\text{SCH}_3)_{18}^-$ (see Fig. S7(b))† which is important because changes in orbital localization and directionality has been shown to contribute to the reactivity of Au clusters.^{69,70}

As a final note, although our results rationalize a series of experimental observations, they are solely based on thermodynamic viewpoints and do not take into consideration kinetic limitations in the form of activation barriers. Barriers for proton-electron transfer in CO_2 reduction to CH_4 and CH_3OH have been calculated on Pt, Cu, and Au surfaces.^{71,72} The calculated barriers for the steps relevant to this study

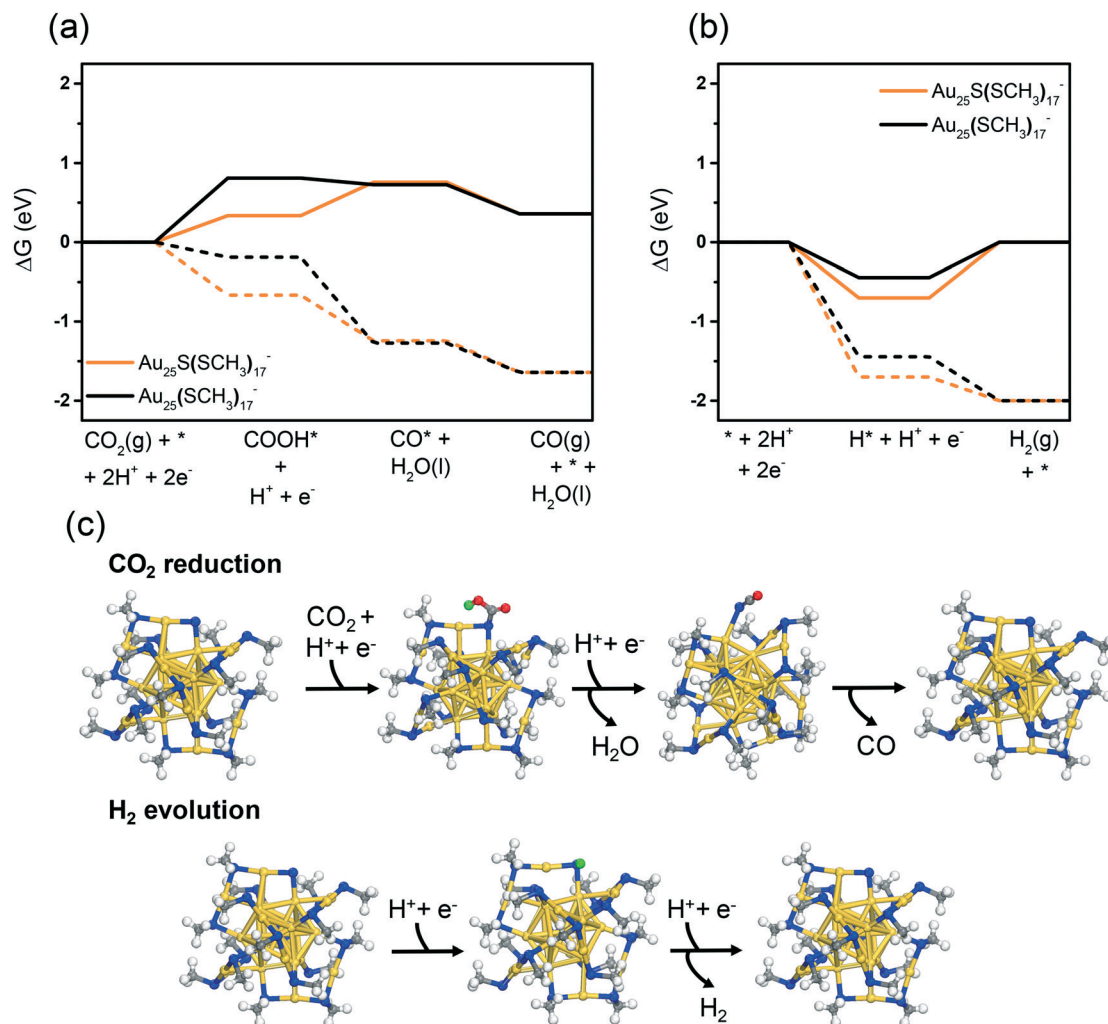


Fig. 7 Free energy diagrams (ΔG) for the (a) reduction of CO_2 to CO and the (b) hydrogen evolution on the $-\text{CH}_3$ removed $\text{Au}_{25}\text{S}(\text{SCH}_3)_{17}^-$ NC and on the $-\text{SCH}_3$ removed $\text{Au}_{25}(\text{SCH}_3)_{17}^-$ NC. The orange and black lines represent the energy diagrams for the $\text{Au}_{25}\text{S}(\text{SCH}_3)_{17}^-$ and $\text{Au}_{25}(\text{SCH}_3)_{17}^-$ NCs, respectively. The solid lines illustrate the energy diagrams at $U = 0$ V, while the dashed lines represent the energy diagrams at an applied potential of $U = -1.0$ V. The color code for (c) the illustrations of CO_2 reduction and H_2 evolution are as described in Fig. 3.

(see eqn (2) and (3)) were less than 1 eV which is surmountable under room temperature at experimentally applied potentials ($U = -1.0$ V). Thus, we would expect the proton-electron transfer barriers for CO_2 reduction on the Au NCs to be thermally accessible at room temperature. Furthermore, assuming the activation energies for the proton-electron transfer steps scale with ΔG_{rxn} , as in the Brønsted-Evans-Po-

lanyi relationship, we would expect the lowest barriers to be observed on the ligand removed NCs.⁷¹ In our future work, we aim to address the detailed kinetic barriers for ligand removal, which appear to be thermodynamically feasible and responsible for converting an inert NC to an active one, as well as to probe the number of ligands a NC can lose while still maintaining structural integrity.

Table 1 Limiting step and potential of the Au_{25} NCs. $\text{H}^+ + \text{e}^-$ omitted for simplicity

	CO_2	$U_{\text{L}}(\text{CO}_2)$	H_2	$U_{\text{L}}(\text{H}_2)$
$\text{Au}_{25}(\text{SCH}_3)_{18}^-$	$\text{CO}_2 + * \rightarrow * \text{COOH}$	-2.01 V	$* \rightarrow * \text{H}$	-1.38 V
$\text{Au}_{25}(\text{SCH}_3)_{18}^0$	$\text{CO}_2 + * \rightarrow * \text{COOH}$	-1.82 V	$* \rightarrow * \text{H}$	-0.96 V
$\text{Au}_{25}(\text{SCH}_3)_{18}^+$	$\text{CO}_2 + * \rightarrow * \text{COOH}$	-1.92 V	$* \rightarrow * \text{H}$	-1.00 V
$\text{Au}_{25}(\text{SCH}_3)_{17}^-$	$\text{CO}_2 + * \rightarrow * \text{COOH}$	-0.81 V	$* \text{H} \rightarrow \text{H}_2(\text{g}) + *$	-0.44 V
$\text{Au}_{25}(\text{SCH}_3)_{17}^0$	$\text{CO}_2 + * \rightarrow * \text{COOH}$	-1.42 V	$* \rightarrow * \text{H}$	-0.02 V
$\text{Au}_{25}(\text{SCH}_3)_{17}^+$	$\text{CO}_2 + * \rightarrow * \text{COOH}$	-1.42 V	$* \text{H} \rightarrow \text{H}_2(\text{g}) + *$	-0.24 V
$\text{Au}_{25}\text{S}(\text{SCH}_3)_{17}^-$	$* \text{COOH} \rightarrow * \text{CO} + \text{H}_2\text{O}(\text{l})$	-0.42 V	$* \text{H} \rightarrow \text{H}_2(\text{g}) + *$	-0.70 V

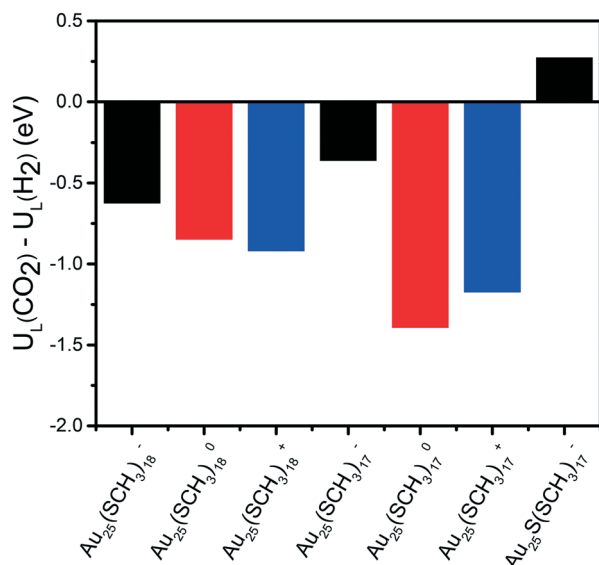


Fig. 8 (a) Difference in limiting potentials of CO₂ reduction and hydrogen evolution ($U_L(\text{CO}_2) - U_L(\text{H}_2)$). The color code represents the three charge states of the Au₂₅ NC (black: negative, red: neutral, blue: positive).

Conclusions

In this work, we applied *ab initio* electronic structure calculations to assess CO₂ reduction and H₂ evolution on fully ligand-protected (Au₂₅(SR)₁₈^q) and partially ligand-removed (removal of -SR and -R) NCs in three charge states $q = -1, 0$, and $+1$. Our results demonstrate that regardless of charge state, the Au₂₅(SR)₁₈^q NC is inactive for CO₂ reduction due to the relative instability of the associated COOH intermediate. On the contrary, our calculations showed that the formation of partially-ligand removed NCs, Au₂₅(SR)₁₇^q ($q = -1, 0, +1$) and Au₂₅S(SR)₁₇⁻, are feasible under reaction conditions. Moreover, Au₂₅(SR)₁₇^q NCs and the Au₂₅S(SR)₁₇⁻ NC stabilized the COOH intermediate more favorably than the Au₂₅(SR)₁₈^q NCs. We therefore conclude that partially-ligand removed clusters, which expose Au and S sites, are the most active for CO₂ reduction under experimentally applied potentials. We found that hydrogen evolution likely competes with CO₂ reduction over the entire potential range of interest. By assessing selectivity, we determined that only the active Au₂₅S(SR)₁₇⁻ NC would be selective towards CO₂ reduction over H₂ evolution. Overall, this work elucidates NC charge state and generation of active surface sites during electrocatalysis as responsible for the stabilization intermediates in CO₂ reduction to CO.

Conflicts of interest

There are no conflicts to declare.

Acknowledgements

GM acknowledges support by the National Science Foundation (NSF, CBET-CAREER program) under Grant No. 1652694.

NA acknowledges support by the NSF Graduate Research Fellowship under Grant No. 1247842. GM and NA would like to acknowledge computational support from the Center for Research Computing and the Extreme Science and Engineering Discovery Environment, which is supported by the NSF (ACI-1548562). R. J. acknowledges financial support from the Air Force Office of Scientific Research under AFOSR Award No. FA9550-15-1-9999 (FA9550-15-1-0154).

References

- 1 IPCC, *Climate Change 2013: The Physical Science Basis. Contribution of Working Group I to the Fifth Assessment Report of the Intergovernmental Panel on Climate Change*, Cambridge University Press, Cambridge, United Kingdom and New York, NY, USA, 2013.
- 2 J. Albo, M. Alvarez-Guerra, P. Castano and A. Irabien, *Green Chem.*, 2015, 17, 2304–2324.
- 3 K. P. Kuhl, E. R. Cave, D. N. Abram and T. F. Jaramillo, *Energy Environ. Sci.*, 2012, 5, 7050–7059.
- 4 A. A. Peterson and J. K. Nørskov, *J. Phys. Chem. Lett.*, 2012, 3, 251–258.
- 5 C. W. Li and M. W. Kanan, *J. Am. Chem. Soc.*, 2012, 134, 7231–7234.
- 6 H. A. Hansen, J. B. Varley, A. A. Peterson and J. K. Nørskov, *J. Phys. Chem. Lett.*, 2013, 4, 388–392.
- 7 J. L. Qiao, Y. Y. Liu, F. Hong and J. J. Zhang, *Chem. Soc. Rev.*, 2014, 43, 631–675.
- 8 B. Khezri, A. C. Fisher and M. Pumera, *J. Mater. Chem. A*, 2017, 5, 8230–8246.
- 9 E. L. Clark, C. Hahn, T. F. Jaramillo and A. T. Bell, *J. Am. Chem. Soc.*, 2017, 139, 15848–15857.
- 10 Gurudayal, J. Bullock, D. F. Sranko, C. M. Towle, Y. W. Lum, M. Hettick, M. C. Scott, A. Javey and J. Ager, *Energy Environ. Sci.*, 2017, 10, 2222–2230.
- 11 X. H. Zhou, R. Liu, K. Sun, Y. K. Chen, E. Verlage, S. A. Francis, N. S. Lewis and C. X. Xiang, *ACS Energy Lett.*, 2016, 1, 764–770.
- 12 A. A. Peterson, F. Abild-Pedersen, F. Studt, J. Rossmeisl and J. K. Nørskov, *Energy Environ. Sci.*, 2010, 3, 1311–1315.
- 13 Y. Hori, *Electrochemical CO2 reduction on metal electrodes*, Springer, New York, 2008.
- 14 D. T. Whipple and P. J. A. Kenis, *J. Phys. Chem. Lett.*, 2010, 1, 3451–3458.
- 15 Y. Hori, K. Kikuchi and S. Suzuki, *Chem. Lett.*, 1985, 1695–1698, DOI: 10.1246/cl.1985.1695.
- 16 H. Mistry, R. Reske, Z. H. Zeng, Z. J. Zhao, J. Greeley, P. Strasser and B. R. Cuenya, *J. Am. Chem. Soc.*, 2014, 136, 16473–16476.
- 17 W. L. Zhu, R. Michalsky, O. Metin, H. F. Lv, S. J. Guo, C. J. Wright, X. L. Sun, A. A. Peterson and S. H. Sun, *J. Am. Chem. Soc.*, 2013, 135, 16833–16836.
- 18 D. R. Kauffman, D. Alfonso, C. Matranga, H. F. Qian and R. C. Jin, *J. Am. Chem. Soc.*, 2012, 134, 10237–10243.
- 19 S. Back, M. S. Yeom and Y. Jung, *ACS Catal.*, 2015, 5, 5089–5096.
- 20 B. Hvolbaek, T. V. W. Janssens, B. S. Clausen, H. Falsig, C. H. Christensen and J. K. Nørskov, *Nano Today*, 2007, 2, 14–18.

- 21 C. Rogers, W. S. Perkins, G. Veber, T. E. Williams, R. R. Cloke and F. R. Fischer, *J. Am. Chem. Soc.*, 2017, **139**, 4052–4061.
- 22 A. S. Hall, Y. Yoon, A. Wuttig and Y. Surendranath, *J. Am. Chem. Soc.*, 2015, **137**, 14834–14837.
- 23 R. C. Jin, H. F. Qian, Z. K. Wu, Y. Zhu, M. Z. Zhu, A. Mohanty and N. Garg, *J. Phys. Chem. Lett.*, 2010, **1**, 2903–2910.
- 24 G. Li and R. C. Jin, *Acc. Chem. Res.*, 2013, **46**, 1749–1758.
- 25 P. Haider, A. Urakawa, E. Schmidt and A. Baiker, *J. Mol. Catal. A: Chem.*, 2009, **305**, 161–169.
- 26 L. D. Menard, F. T. Xu, R. G. Nuzzo and J. C. Yang, *J. Catal.*, 2006, **243**, 64–73.
- 27 Z. L. Wu, D. E. Jiang, A. K. P. Mann, D. R. Mullins, Z. A. Qiao, L. F. Allard, C. J. Zeng, R. C. Jin and S. H. Overbury, *J. Am. Chem. Soc.*, 2014, **136**, 6111–6122.
- 28 D. R. Kauffman, J. Thakkar, R. Siva, C. Matranga, P. R. Ohodnicki, C. J. Zeng and R. C. Jin, *ACS Appl. Mater. Interfaces*, 2015, **7**, 15626–15632.
- 29 D. R. Kauffman, D. Alfonso, C. Matranga, P. Ohodnicki, X. Y. Deng, R. C. Siva, C. J. Zeng and R. C. Jin, *Chem. Sci.*, 2014, **5**, 3151–3157.
- 30 D. R. Alfonso, D. Kauffman and C. Matranga, *J. Chem. Phys.*, 2016, **144**, 184705.
- 31 S. Zhao, N. Austin, M. Li, Y. Song, S. D. House, S. Bernhard, J. C. Yang, G. Mpourmpakis and R. Jin, *ACS Catal.*, 2018, **8**, 4996–5001.
- 32 X. T. Nie, H. F. Qian, Q. J. Ge, H. Y. Xu and R. C. Jin, *ACS Nano*, 2012, **6**, 6014–6022.
- 33 G. Centi, E. A. Quadrelli and S. Perathoner, *Energy Environ. Sci.*, 2013, **6**, 1711–1731.
- 34 X. Chen and H. Hakkinen, *J. Am. Chem. Soc.*, 2013, **135**, 12944–12947.
- 35 G. Li, H. Abroshan, Y. X. Chen, R. C. Jin and H. J. Kim, *J. Am. Chem. Soc.*, 2015, **137**, 14295–14304.
- 36 S. Das, A. Goswami, M. Hesari, J. F. Al-Sharab, E. Mikmekova, F. Maran and T. Asefa, *Small*, 2014, **10**, 1473–1478.
- 37 J. Fang, J. G. Li, B. Zhang, X. Yuan, H. Asakura, T. Tanaka, K. Teramura, J. P. Xie and N. Yan, *Nanoscale*, 2015, **7**, 6325–6333.
- 38 J. A. Lopez-Sanchez, N. Dimitratos, C. Hammond, G. L. Brett, L. Kesavan, S. White, P. Miedziak, R. Tiruvalam, R. L. Jenkins, A. F. Carley, D. Knight, C. J. Kiely and G. J. Hutchings, *Nat. Chem.*, 2011, **3**, 551–556.
- 39 B. Zhang, S. Kaziz, H. Li, M. G. Hevia, D. Wodka, C. Mazet, T. Burgi and N. Barrabes, *J. Phys. Chem. C*, 2015, **119**, 11193–11199.
- 40 E. Andrews, S. Katla, C. Kumar, M. Patterson, P. Sprunger and J. Flake, *J. Electrochem. Soc.*, 2015, **162**, F1373–F1378.
- 41 J. A. Trindell, J. Clausmeyer and R. M. Crooks, *J. Am. Chem. Soc.*, 2017, **139**, 16161–16167.
- 42 J. P. Perdew, K. Burke and M. Ernzerhof, *Phys. Rev. Lett.*, 1996, **77**, 3865–3868.
- 43 J. VandeVondele and J. Hutter, *J. Chem. Phys.*, 2007, **127**, 114105.
- 44 S. Goedecker, M. Teter and J. Hutter, *Phys. Rev. B: Condens. Matter Mater. Phys.*, 1996, **54**, 1703–1710.
- 45 J. VandeVondele, M. Krack, F. Mohamed, M. Parrinello, T. Chassaing and J. Hutter, *Comput. Phys. Commun.*, 2005, **167**, 103–128.
- 46 Y. G. Wang, Y. Yoon, V. A. Glezakou, J. Li and R. Rousseau, *J. Am. Chem. Soc.*, 2013, **135**, 10673–10683.
- 47 C. Y. Liu, Y. Z. Tan, S. S. Lin, H. Li, X. J. Wu, L. Li, Y. Pei and X. C. Zeng, *J. Am. Chem. Soc.*, 2013, **135**, 2583–2595.
- 48 L. Ma, K. Laasonen and J. Akola, *J. Phys. Chem. C*, 2017, **121**, 10876–10886.
- 49 M. Prakash, K. Mathivon, D. M. Benoit, G. Chambaud and M. Hochlaf, *Phys. Chem. Chem. Phys.*, 2014, **16**, 12503–12509.
- 50 Y. G. Wang, D. H. Mei, V. A. Glezakou, J. Li and R. Rousseau, *Nat. Commun.*, 2015, **6**, 6511.
- 51 M. Zhu, C. M. Aikens, F. J. Hollander, G. C. Schatz and R. Jin, *J. Am. Chem. Soc.*, 2008, **130**, 5883–5885.
- 52 G. Li, H. Abroshan, C. Liu, S. Zhuo, Z. M. Li, Y. Xie, H. J. Kim, N. L. Ros and R. C. Jin, *ACS Nano*, 2016, **10**, 7998–8005.
- 53 J. K. Nørskov, J. Rossmeisl, A. Logadottir, L. Lindqvist, J. R. Kitchin, T. Bligaard and H. Jonsson, *J. Phys. Chem. B*, 2004, **108**, 17886–17892.
- 54 J. B. Varley, H. A. Hansen, N. L. Ammitzboll, L. C. Grabow, A. A. Peterson, J. Rossmeisl and J. K. Nørskov, *ACS Catal.*, 2013, **3**, 2640–2643.
- 55 D. F. Gao, H. Zhou, J. Wang, S. Miao, F. Yang, G. X. Wang, J. G. Wang and X. H. Bao, *J. Am. Chem. Soc.*, 2015, **137**, 4288–4291.
- 56 S. A. Akhade, W. J. Luo, X. W. Nie, A. Asthagiri and M. J. Janik, *Catal. Sci. Technol.*, 2016, **6**, 1042–1053.
- 57 A. Venzo, S. Antonello, J. A. Gascon, I. Guryanov, R. D. Leapman, N. V. Perera, A. Sousa, M. Zamuner, A. Zanella and F. Maran, *Anal. Chem.*, 2011, **83**, 6355–6362.
- 58 M. Z. Zhu, C. M. Aikens, M. P. Hendrich, R. Gupta, H. F. Qian, G. C. Schatz and R. C. Jin, *J. Am. Chem. Soc.*, 2009, **131**, 2490–2492.
- 59 M. Z. Zhu, W. T. Eckenhoff, T. Pintauer and R. C. Jin, *J. Phys. Chem. C*, 2008, **112**, 14221–14224.
- 60 G. Periyasamy, E. Durgun, J. Y. Raty and F. Remacle, *J. Phys. Chem. C*, 2010, **114**, 15941–15950.
- 61 J. A. Keith and E. A. Carter, *J. Chem. Theory Comput.*, 2012, **8**, 3187–3206.
- 62 K. Chan, C. Tsai, H. A. Hansen and J. K. Nørskov, *ChemCatChem*, 2014, **6**, 1899–1905.
- 63 H. F. Qian, M. Y. Sfeir and R. C. Jin, *J. Phys. Chem. C*, 2010, **114**, 19935–19940.
- 64 J. Akola, M. Walter, R. L. Whetten, H. Häkkinen and H. Grönbeck, *J. Am. Chem. Soc.*, 2008, **130**, 3756–3757.
- 65 X. Hong, K. R. Chan, C. Tsai and J. K. Nørskov, *ACS Catal.*, 2016, **6**, 4428–4437.
- 66 D. Kim, C. L. Xie, N. Becknell, Y. Yu, M. Karamad, K. Chan, E. J. Crumlin, J. K. Nørskov and P. D. Yang, *J. Am. Chem. Soc.*, 2017, **139**, 8329–8336.

- 67 M. R. Singh, E. L. Clark and A. T. Bell, *Phys. Chem. Chem. Phys.*, 2015, **17**, 18924–18936.
- 68 S. Zhao, R. X. Jin, Y. B. Song, H. Zhang, S. D. House, J. C. Yang and R. C. Jin, *Small*, 2017, **13**, 7.
- 69 S. Chretien, S. K. Buratto and H. Metiu, *Curr. Opin. Solid State Mater. Sci.*, 2007, **11**, 62–75.
- 70 G. Mpourmpakis, A. N. Andriotis and D. G. Vlachos, *Nano Lett.*, 2010, **10**, 1041–1045.
- 71 C. Shi, K. Chan, J. S. Yoo and J. K. Norskov, *Org. Process Res. Dev.*, 2016, **20**, 1424–1430.
- 72 X. W. Nie, W. J. Luo, M. J. Janik and A. Asthagiri, *J. Catal.*, 2014, **312**, 108–122.